2011

Stress analysis of welded gusseted frames

Zamir Imtiyaz Syed
Iowa State University

Stress analysis of welded gusseted frames

by

Zamir Imtiyaz Syed

A thesis submitted to the graduate faculty

in partial fulfillment of the requirements for the degree of

MASTER OF SCIENCE

Major: Mechanical Engineering

Program of Study Committee:
Palaniappa A. Molian, Major Professor
Pranav Shrotriya
Fouad Fanous

Iowa State University

Ames, Iowa

2011

Table of Contents

List of Figures

Abstract

Welded gusseted frame design for fatigue loading is largely not addressed in modern machine design texts. This research intends to uncover stress solutions for critical locations on welded gusseted frames so that such a common engineering structure can have design basis. The problem was approached using static equilibrium relations to populate coefficients of deliberately chosen line stress functions. The results from that analysis were used in a subsequent fracture mechanics analysis to develop the singular stress field at a weld toe. The current research resulted in solutions for the two most critical stress states on welded gusseted frame structures.

Chapter 1: Introduction

1.1 Problem Definition

Gusseted frames are a common subject in mechanical design. Frames are generally beam-based structures where the connection between beams is a moment carrying connection. The use of gussetry in mechanical design is intended save material by allowing the reduction of the cross-section of at least one beam in a frame connection. Examples of gusseted frames are shown in the following figures.

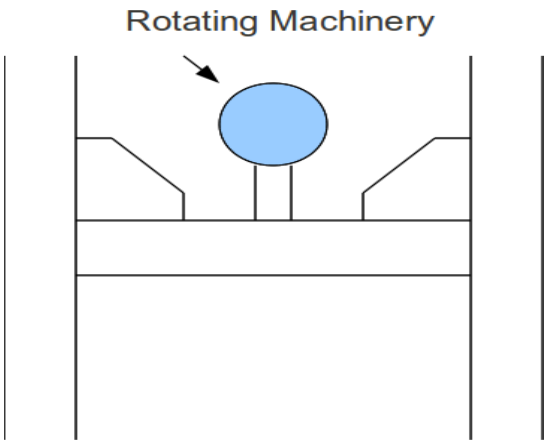

Figure 1.1: Gusseted frame example. Rotating machinery supported by gusseted frame

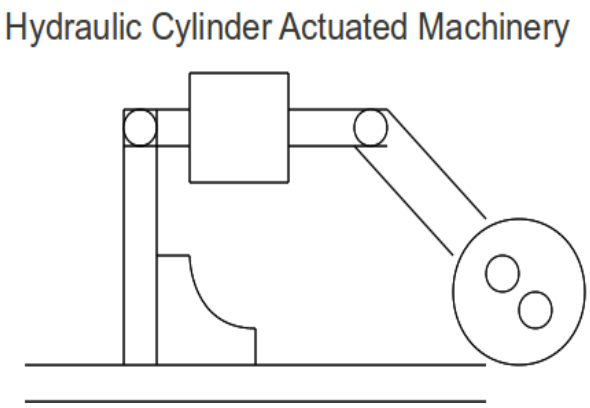

Figure 1.2: Gusseted frame example. Hydraulic cylinder actuated mechanism or machinery

Despite the common uses of gusseted frames, current design and analysis literature does not address this topic from a structural failure perspective. Gaps in the literature exist for in-plane loading of finite

parabolic plates, as well as for the contact problem of finite parabolic plates with beams. The literature also lacks weld metal mechanical properties for many common combinations of base metal and weld metal. In particular, elastic material properties of MIG/MAG welded mild steel are not present. Because the aforementioned items are not available in the literature, a stress analysis at the toe of a welded connection is not possible. Consequently, fatigue failure criterion for welded connections cannot be applied to gusseted frame connections without significant effort in numerical simulation or physical testing.

A very simple mechanical frame consisting of two beams and one moment connection should be the focus when moving towards a reliable method to determine frame stresses. Therefore the problem is constructed as such: Two welded beams are oriented 90 degrees from each other. One beam is cantilevered and the other is loaded at its tip. The addition

of a gusset is provided at the joint. It is desired that the service life of the frame be determined through the use of common fatigue algorithms. See figure 1.3 for clarity on the geometry of the problem.

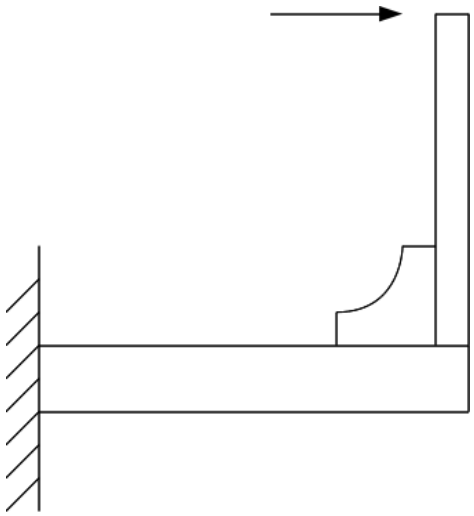

Figure 1.3: Problem definition

1.2 Objective

The objective of this paper is to create useful stress results in critical locations on the gusseted frame that can serve as inputs into a fatigue model.

1.3 Organization of Sections

This paper consists of six main sections outside of this introduction. The first section is dedicated to exposing the existing literature on in-plane stress analysis in beams, plates, and contact problems. The second section develops the methodology for finding the critical stresses in a gusseted frame. The third section provides experimental results for Young's modulus of weld metal, as well as a discussion about the literature on material property acquisition. The fourth section provides a stress analysis for the critical near-field region of the gusset tip. The fifth section details an effective design plan to use the

results of this research, as well as a worked example. The sixth section comments on several possibilities on expanding the methodology to approach other complex geometries that require frequent stress analysis. Conclusions based on the current project are also discussed.

Chapter 2: Background

In order to develop the necessary critical stress states on gusseted frames, a thorough analysis of existing literature is most appropriate. In particular, 'T' joints and beam-plate interactions, as well as plane elasticity literature are important to this research.

Literature on T or L joints is limited. The vast majority of studies regarding the stress distributions in T joints have been performed using finite element analysis (FEA) [N'Diaye, et al, 2009]. Analytical solutions are much more difficult to come by. This is perhaps because the function of contact stress is largely unknown, therefore, difficult variational calculus methods are often used for an exact solution. Solutions for mixed problems in elasticity do well in capturing complete stress distributions in all participating mechanical elements. Popov and Tikhonenko [1974] finds the exact solution for a semi-infinite beam bonded to an elastic wedge. In a separate paper, Popov and Tikhonenko [1975] find a similar solution for two beams in contact with a wedge. These solutions utilize the calculus of variations where the contact interface is the unknown functional. This paper would like to deviate from the variational calculus approach and assume a contact stress function which can be determined from either observation or some other concept in analytical mechanics. Concepts in elasticity such as peeling stress, elastic mismatch stress, and the stress field due to corner and free edge singularities present local varying stress fields that are dependent on local geometry, material properties, and local nominal stress fields. They can be used to fulfill the unknown contact stress requirement. These varying stress fields could be superimposed

on the nominal stress fields from plane stress and beam solutions to potentially guide the design process. A discussion about each of these stress concepts will follow.

This paper will draw upon work from several areas of study in mechanics. Each element in the T or L joint has easily calculated nominal stress distributions. The basic beam stresses and deflections can be determined from a simple strength of materials approach [Hibbeler, 2005]. The various gusset plates used in this paper will be sufficiently thin so that plane stress conditions can be assumed. For a simple straight sided gusset plate, Airy's stress function can be used to develop the 2-D plane stress distribution [Timoshenko, 1951]. Airy's stress formulations for plane problems involves directly integrating stresses rather than displacements to find equilibrium within the confines of prescribed boundary conditions. This is the preferred method when solving plane problems. However, for more complicated gusset geometries, such as the finite gusset with a parabolic free edge, more complicated methods must be employed. Variational techniques or conformal mapping of complex potentials onto multiple polar coordinate systems would have to be developed for an exact solution of stress distribution. An advanced mathematical background and extremely developed mechanical insight, not to mention and enormous time investment, is required for such a solution. It does not offer significant advantages over a reasonable estimate of the maximum stress on the parabolic free edge.

The interaction between the bonded beams (T or L joint) can potentially be studied from the perspective of peeling or cleavage stresses. Peeling stress concepts came about in the study of adhesively bonded joints. Kaelble [1960] develops the theory for peeling stresses and provides experimental results to verify his findings. Peeling or

cleavage occurs when forces act on a joint as to pry or peel the joint apart. It is a widely used theory in adhesive-bonded joint design. The interfacial stresses provided by peeling stress theory can potentially help quantify local stress singularities at free edges at bonded interfaces. Numerical studies of cleavage stress distributions are shown in Kong, You, Zheng and Yu, [2007], these results clearly show the contribution of peeling to the entire stress state of a joint. Malek, Hamed and Ehsani [1998] apply the fundamentals of peeling stress concepts to a uniform beam reinforced by a uniform plate. The solution is derived from elasticity principles. While the result of this analysis is not practical for use in gusseted joint design, the methodology is very telling. This method is extended in [Stratford and Cadei, 2006] where non uniform reinforcing plates are considered. However, as mentioned in [Stratford and Cadei, 2006], the problem becomes complicated enough that an analytical solution is no longer practical or useful. The study resorts to numerical studies to quantify peeling stresses. Methods of quantifying the varying stiffness of the reinforcing plate is how Stratford and Cadei [2006] becomes useful to this project. A large time frame in this study was dedicated to finding a peeling stress result for the interfacial effects of beam bending stresses; however, it was concluded here, like in Stratford and Cadie [2006], that a peeling stress result is not possible to attain for small beam sections. In this author's perspective, a peeling stress solution to the problem of a welded T or L joint would be optimal because it would provide a complete interfacial normal and shear stress distribution. However, developing boundary conditions for the complementary solution for peeling stresses becomes very difficult. The normal stress distribution of peeling stresses for semi-infinite beams follows some variation of the fundamental solution for fourth order differential equations where the (x=0) occurs at the

free edge of the beams and -x corresponds to the longitudinal ordinate into the beam space. In past peeling stress results, it was assumed that the normal stress at the interface went to zero as x tended towards negative infinity. Therefore, the final term in the complementary solution was dropped. This simplified the problem greatly. The two remaining boundary conditions were formulated using known values for shear stress at the interface [Malek, Hamed and Ehsani, 1998]. Dropping the final term in the complementary solution is not possible for finite, and more specifically, small, beam sections because the peeling stress result does not have enough longitudinal space to return to a uniform value equal to beam bending stress. From observation of many FE models, the normal stress at the opposite free edge ($x = x_{end}$) is some superposition of nominal bending stresses and peeling stress effects. Unfortunately, this is unknown and can no longer be used as a boundary condition. The peeling stress problem returns to an under-defined state. When considering a gusset reinforced T/L joint, the boundary conditions become further complicated because the variation of stiffness of the gusset and beam combination is a function of longitudinal distance.

Given the background on contact stresses and finite plates with irregular geometry, the subsequent analysis is used to develop a contact stress function and an estimate for stresses in a finite gusset with a parabolic free edge. The contact stress function is assumed to be cubic in nature. It does not include the singularity at the free edge. The singularity will be discussed in chapter 5.

Chapter 3: Problem Formulation and Solution

The problem defined in section 1.1 will be formulated here. A solution is drawn from existing work, equilibrium relations, and stiffness considerations.

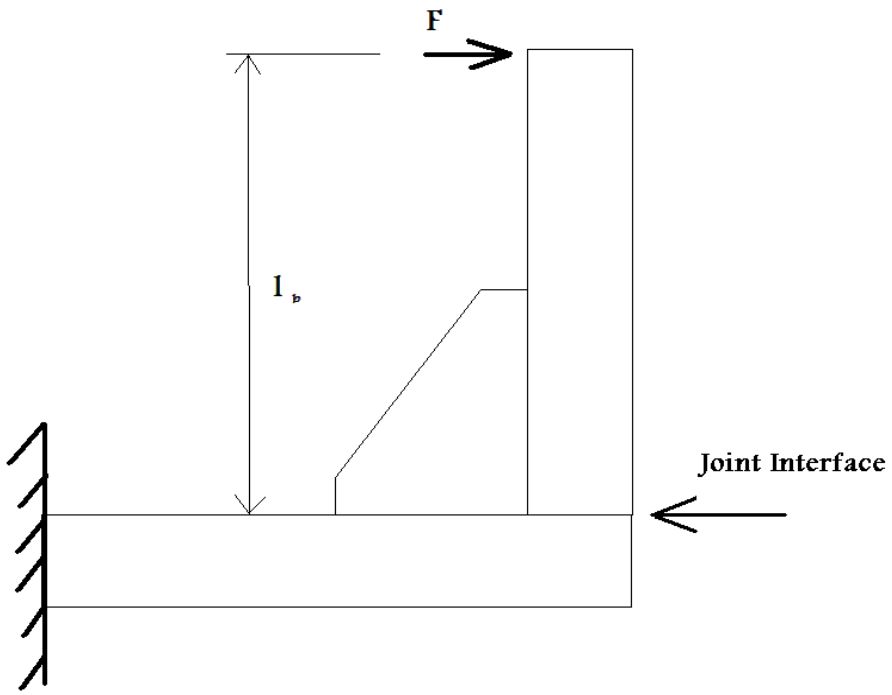

Figure 3.1: Gusseted joint.

A gusseted joint is shown in figure 3.1. The joint is cut at the joint interface.

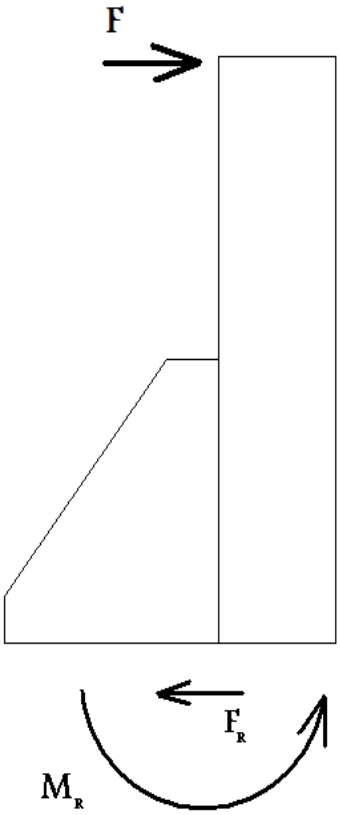

Figure 3.2: Frame cut at joint interface.

Figure 3.2 serves as the free body diagram for this problem. From this point in this analysis, it is assumed that l_b is sufficiently large and F_R will be neglected because M_R will dominate the stress state at the interface. The stress distribution at the interface will be primarily determined by M_R. In this case, $M_R = F \times l_b$.

Observing the cross section taken at the cut, it is easy to separate the joint interface into two elements: the beam interface and the gusset interface. The beam interface has an area moment of inertia of I_b about its neutral axis at the ordinate of $y = -y_1$, and an area of A_1. The gusset interface has an area moment of inertia of I_g about its neutral axis at $y = y_2$, and an area of A_2.

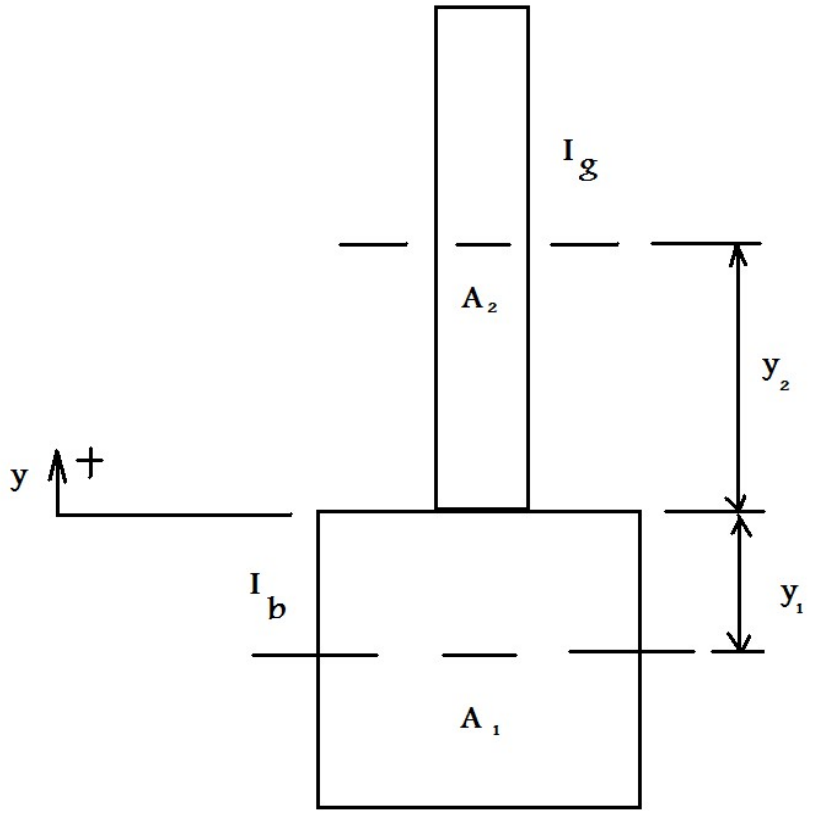

Figure 3.3: Cross section of interface.

To proceed, it is necessary to find the neutral axis of the entire cross section. From elementary mechanics it is known that

$$y_{neutral} \sum A_n = \sum y_n A_n \quad \text{therefore,}$$

$$(1) \quad y_3 = \frac{\sum y_n A_n}{\sum A_n} = \frac{y_1 A_1 + y_2 A_2}{A_1 + A_2}$$

noting that y_1 has a negative value associated with it.

y_3 = neutral axis ordinate for entire cross section.

It is also necessary to determine the area moment of inertia for the entire interface. Using the parallel axis theorem, it is known that

$$(2) \quad I_{total} = I_b + A_1(y_1 - y_3)^2 + I_g + A_2(y_2 - y_3)^2$$

noting that y_1 is typically negative.

It is now possible to capture the nominal bending stress distribution. By the strength of materials approach, bending stress S_b is

$$S_b(y) = \frac{M_R(y - y_3)}{I_{total}} \quad \text{where } -h_1 \le y \le h_2.$$

h_1 and h_2 are defined as the height of each elemental cross section. See figure 3.4 for further clarification.

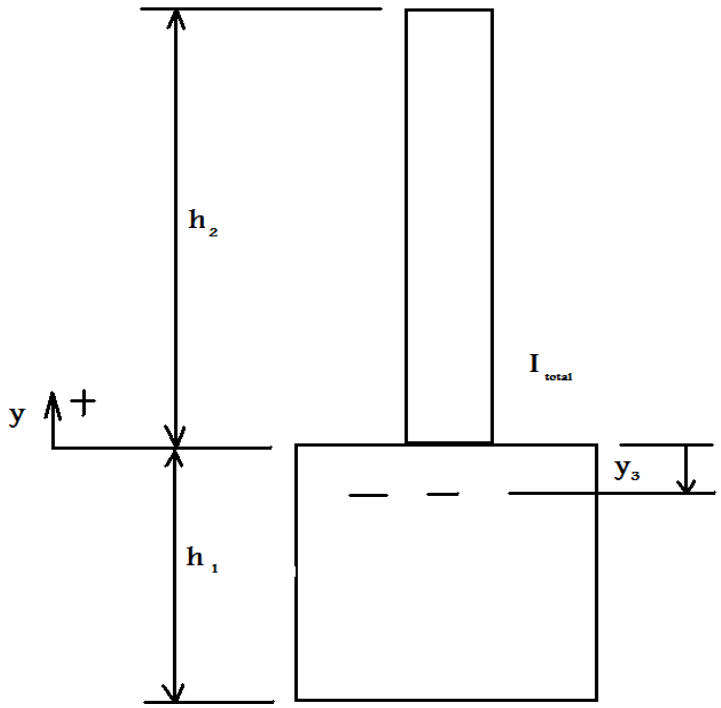

Figure 3.4: View of cross section with all relevant geometric parameters for stress distribution calculation.

The stress distribution over the gusset element will be defined by

$$(3) \quad S_b(y) = \frac{M_R(y - y_3)}{I_{total}} \quad \text{where } 0 \le y \le h_2.$$

The stress distribution over the beam cross section will be defined by

$$(4) \quad S_b(y) = \frac{M_R(y - y_3)}{I_{total}} \quad \text{where } -h_1 \leq y \leq 0.$$

Note that y_3 can be negative given the working coordinate system described in figure 4. By observing many beam-gusset interfaces in FE models, it is noticed that the stress distribution in the gusset section of the interface does *not* behave as described in equation (3). The stress distribution in the gusset at the interface changes as the profile of the gusset changes. The various gussets available to engineers provide stress distributions that can be approximated by using a variation of the stiffness method. The stress distribution is characterized in three steps. The first step is assuming a load path through the gusset plane. The second step is establishing equilibrium. The third step is solving for the interfacial stress distribution.

Step 1: Assume load path through the gusset

It is possible to assume a reasonably accurate load path through a gusset. The distribution of stresses in a wedge has been developed [Timoshenko and Goodier, 1951]. The results from that analysis can be used to approximate a load path. It is seen that stress flows in a radial path about R=0 (see figure 3.5). To make this useful, the length of the paths need to be quantified so that ratios of pseudo stiffness can be developed. The stiffness of an axially loaded bar is:

$$k = \frac{AE}{L}$$

where A = area, E = elastic modulus, and L = length of bar.

For the purposes of this analysis, take L to be the length of the radial load path instead of the length of a bar. Since the thickness of the gusset is assumed to be uniform, A is

removed from the analysis. The material properties of the gusset are also assumed constant, therefore, E is set to unity. The equation for stiffness reduces to (5).

$$(5) \quad k = \frac{1}{r\Phi}$$

where r = radial coordinate on gusset, ϕ = angular range. r and ϕ are clarified in figure 3.5.

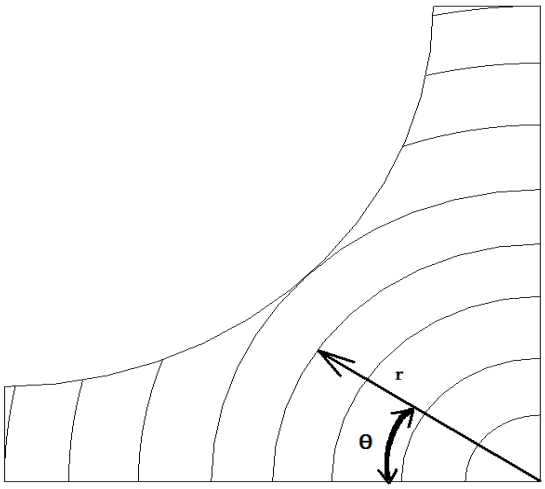

Figure 3.5: Gusset with radial stress contours.

The previous formulation for stiffness presents problems near the free edges of the gusset where the radial lines are no longer continuous on the gusset. The limiting case for this simple formulation is when a radial stress contour line is tangent with the free edge nearest to the origin. In the case of a typical straight-edged gusset that is symmetrical about $\theta = \pi/4$, the limiting case is defined as r_L in (6).

$$(6) \quad r_L = \sqrt{\frac{(l_{leg} + l_{tip})^2}{2}}$$

Where l_{leg} and l_{tip} are defined in figure 6.

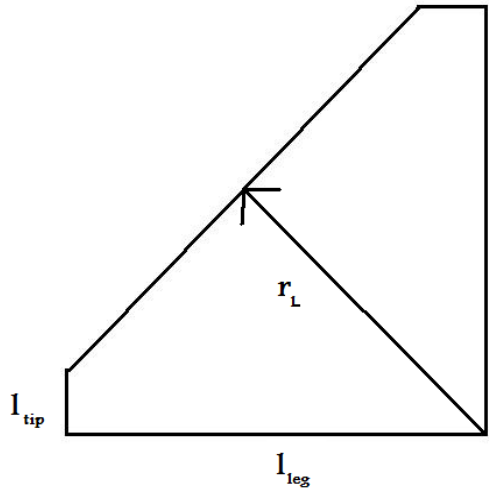

Figure 3.6: Straight-edged gusset with referenced parameters defined.

The load path length for a longest radial contour line is given by (7).

$$k_L = \frac{1}{r_L \frac{\pi}{2}} \quad (7)$$

In the case of a parabolic gusset, the limiting radius is given in (8).

$$r_L = \sqrt{2 l_{leg}^2} - r_p \quad (8)$$

where the appropriate parameters are defined in figure 7. The stiffness of the load path is calculated the same way as in the straight-edged gusset case, except that r_L from (8) is substituted into (7).

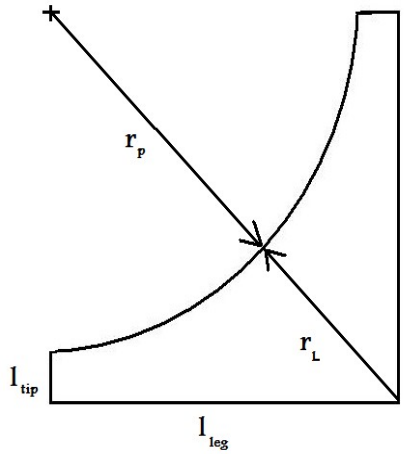

Figure 3.7: Parabolic gusset with referenced parameters defined.

When $r > r_L$, the load path becomes slightly more complicated. When a free edge obstructs a load path, it serves as the new load path until the radial line re-enters the gusset material space. An example of this is shown (figure 3.8) for a case of a parabolic gusset where the example load path is at

$r = l_{leg}$.

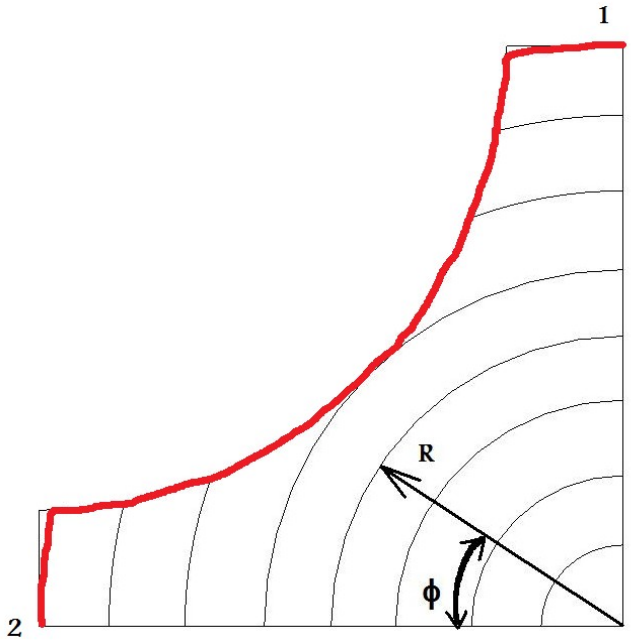

Figure 3.8: The load path at R = l_{leg} is shown in red. The radial contour line is followed wherever possible except for where a free edge serves as the load path.

The length of the load path at R = l_{leg} needs to be quantified. For the case of the straight-edged gusset where r_2 is the equation for the long diagonal free edge on the gusset,

$$(9)\quad r_2=\sqrt{\frac{(l_{leg}+l_{tip})^2}{2}}\,sec\,(\theta-\frac{\pi}{4})$$

To solve for θ in (9) where r_2 intersects $r_1 = l_{leg}$, (r_1 is the radius of longest load path), take

$$r_2=r_1=l_{leg}$$

Solving for θ from (9):

$$(10)\quad \theta_1,\theta_2=\frac{\pi}{4}\pm\arccos\left(\frac{1}{l_{leg}}\sqrt{\frac{1}{2}(l_{leg}+l_{tip})^2}\right)$$

To find the length of the load path, D_1, at $r_1 = l_{leg}$, geometric relations are used. The result is (11).

$$(11)\quad D_1=2\,l_{leg}\,\theta_1+\sqrt{(2\,l_{leg}^2-2\,l_{leg}^2\cos(\theta_1-\theta_2))}$$

therefore, the stiffness of this load path is given by (12).

$$(12)\quad k_{end}=\frac{1}{D_1}$$

For the case of the parabolic gusset, similar steps are employed as in the load path formulation for the straight-edged gusset. In this case, the equation for the parabolic free edge, r_3, is given by the solution of:

$$(13)\quad r_3^2-2\,r_3\,r_0\cos\left(\theta-\frac{\pi}{4}\right)+r_0^2=r_p^2$$

where $r_p=l_{leg}-l_{tip}$ (see figure 3.7), and $r_0=l_{leg}\sqrt{2}$

The load path radius is set equal to r_3,

$$r_3=r_1=l_{leg}$$

Solving (13) for θ,

$$(14)\quad \theta_3,\theta_4=\frac{\pi}{4}\pm\arccos\left(\frac{r_3^2-(l_{tip}-l_{leg})^2+r_0^2}{2\,r_3\,r_0}\right)$$

Using the result for θ, the load path length, D_2, for $r_1 = l_{leg}$ is given by (15).

$$(15)\quad D_2=2\,l_{leg}\,\theta_3+r_p(\theta_3-\theta_4)$$

therefore, the stiffness for this load path is given in (16) using D2 from (15).

$$(16)\quad k_{end}=\frac{1}{D_2}$$

The results for k_L and k_{end} will become useful later in this analysis.

Step 2: Establishing equilibrium.

Recall that the bending stress at the beam-gusset interface was described in the strength of materials context as being linearly distributed over the entire section. It was argued

that this is not an entirely true representation of the stress distribution in the gusset space. However, it is observed that this is mostly accurate in the beam space. This can be used to help develop the stress distribution in the gusset space.

Recall, $S_b = \frac{M_R(y - y_3)}{I_{total}}$ Where $0 \leq y \leq -h_1$, is the stress distribution over the beam space.

Integrating the bending stress over the beam space will result in the total resultant force acting in the beam space. The magnitude of the total stress in the gusset space must equal the total stress in the beam space; it must also act in the opposite direction to maintain a force equilibrium.

$$(17) \quad F_{resultant} = \int S_b \, dA_1$$

The interface region must also maintain a rotational equilibrium about the neutral axis. Therefore, the moment caused by the stress distribution in the beam space must equal the moment acting in the gusset space of the interface. This enforces the force equilibrium condition as well as the moment equilibrium condition. Integrating for the total moment across the beam space results in (18).

$$(18) \quad M_{resultant} = \int S_b \, y \, dA_1$$

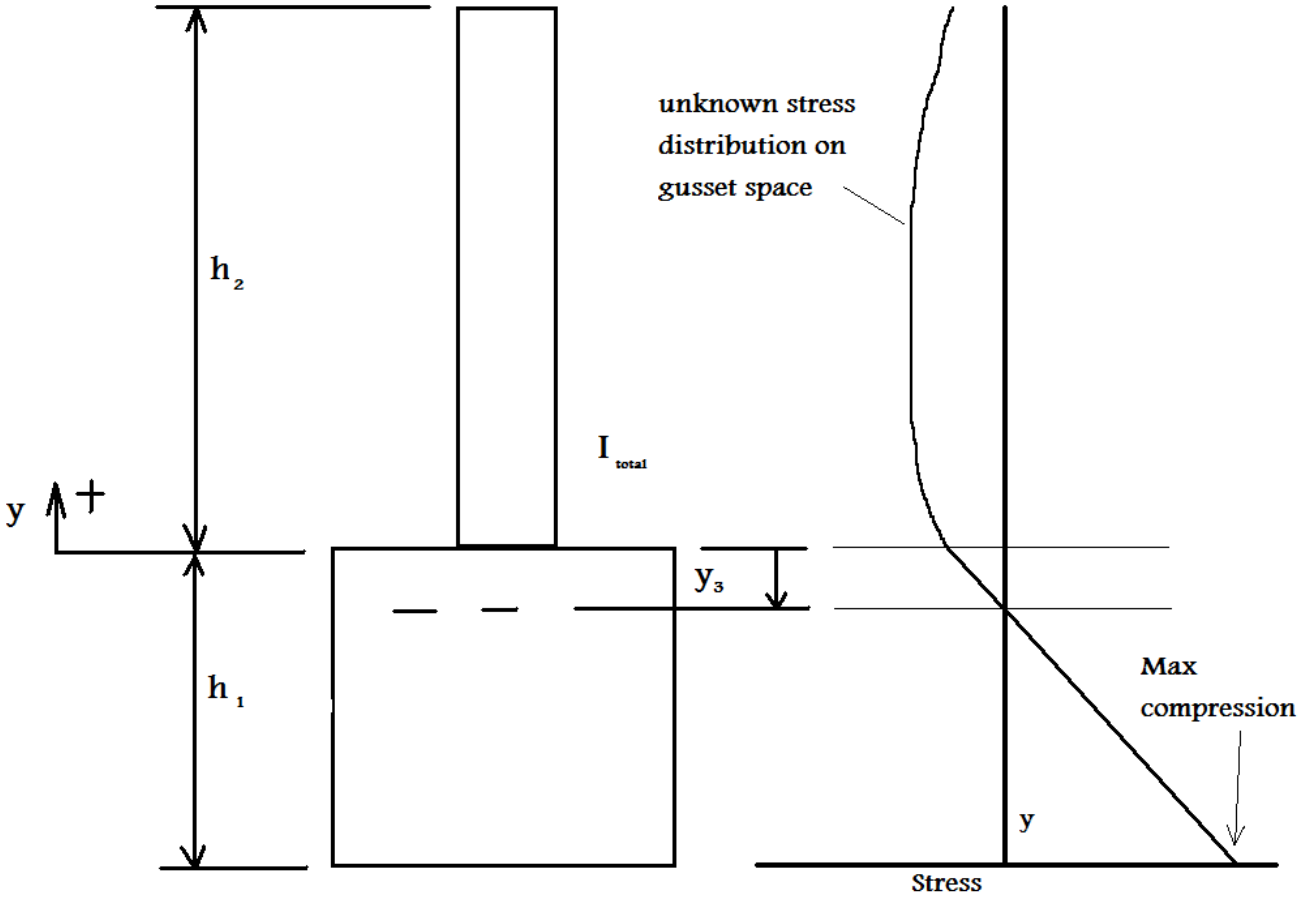

Figure 3.9: The stress distribution across the interface.

Step 3: Solving for angular gusset stress distribution at interface.

A stress function for the gusset space of the interface is proposed in simple cubic form.

$$(19) \quad S_g = My^3 + Ny^2 + O\,y + P$$

The unknown coefficients M, N, and O can be solved for by using the equilibrium and stiffness relations developed in the previous sections, as well as the known stress at y = 0. The following system of equations is used to solve for the coefficients.

First,

$$(20) \quad S_g(y=0) = S_b(y=0) = P$$

$\int S_g\,dA_g = F_{res}$ where A_g is the area of the gusset at the interface; gusset thickness, t, is assumed to be uniform, therefore, from (17):

$$(21) \quad \frac{h_2\,t}{12}(3\,M\,h_2^3 + 4\,N\,h_2^2 + 6\,O\,h_2 + 12\,P) = F_{res}$$

$\int S_g\,x\,dA_g = M_{res}$ where A_g is the area of the gusset at the interface; gusset thickness, t, is assumed to be uniform, therefore, from (18):

$$(22) \quad \frac{h_2^2\,t}{60}(12\,M\,h_2^3 + 15\,N\,h_2^2 + 20\,O\,h_2 + 30\,P) = M_{res}$$

and from the stiffness relations (7) and (12) or (16):

$$(23) \quad \frac{k_L}{k_{end}} = \frac{S_g(y=r_L)}{S_g(y=h_2)} = \frac{M\,r_L^3 + N\,r_L^2 + O\,r_L + P}{M\,h_2^3 + N\,h_2^2 + O\,h_2 + P}$$

Solving for M,N, and O (eqns. 24,25, 26):

$$M=\frac{-5(12M_{res}h_2^2k_L+12M_{res}k_{end}r_L^2-24M_{res}h_2k_Lr_L-3Ph_2^4k_Lt-3Ph_2^4k_{end}t+4Ph_2^3k_Lr_Lt+8Ph_2^3k_{end}r_Lt-6Ph_2^2k_{end}r_L^2t)}{h_2^3t(3h_2^4k_L-20k_{end}r_L^4+15h_2^2k_Lr_L^2-12h_2^2k_{end}r_L^2-16h_2^3k_Lr_L+30h_2k_{end}r_L^3)}$$

$$N=\frac{6(10M_{res}h_2^3k_L+20M_{res}k_{end}r_L^3-30M_{res}h_2k_Lr_L^2-3Ph_2^5k_Lt-2Ph_2^5k_{end}t+5Ph_2^3k_Lr_L^2t-10Ph_2^2k_{end}r_L^3t+10Ph_2^3k_{end}r_L^2t)}{h_2^3t(3h_2^4k_L-20k_{end}r_L^4+15h_2^2k_Lr_L^2-12h_2^2k_{end}r_L^2-16h_2^3k_Lr_L+30h_2k_{end}r_L^3)}$$

$$O=\frac{3r_L(40M_{res}h_2^3k_L+20M_{res}k_{end}r_L^3-60M_{res}h_2^2k_Lr_L-12Ph_2^5k_Lt-8Ph_2^5k_{end}t+15Ph_2^4k_Lr_Lt+15Ph_2^4k_{end}r_Lt-10Ph_2^2k_{end}r_L^3t)}{h_2^3t(3h_2^4k_L-20k_{end}r_L^4+15h_2^2k_Lr_L^2-12h_2^2k_{end}r_L^2-16h_2^3k_Lr_L+30h_2k_{end}r_L^3)}$$

By substituting (24), (25), and (26) into (19), the angular gusset interface stress distribution (not including corner stress intensities) is now fully characterized by S_g. The angular stress at the tip of the gusset is given in (27).

$$(27)\quad S_{tip}=S_g(y=l_{leg})$$

The stress at the limiting radial line is the maximum stress in the cubic distribution. It is given by (28).

$$(28)\quad S_{rL}=S_g(y=r_L)$$

This characterizes the stress distribution over the beam-gusset interface. There is another critical stress area on typical gusseted frames that needs to be checked. Referring to figure 3.8, the normal stress on the parabolic free edge of the gusset at $\theta = 45$ degrees is often critical in low-cycle fatigue. It can also be critical if gusset materials are too thin. The angular stress distribution about an axis defined at $\theta = 45$ degrees is observed to be very linear. A linear stress function is assumed for the angular stresses on this axis.

$$(29)\quad S_{45}=Ir+J$$

Where I, J are arbitrary coefficients and r is the radial coordinate referring to figure 3.8.

As shown previously, the stress at the origin is equal to the maximum beam stress in the beam 1. However, due to the orientation of the angular stresses, it is necessary to transform the bending stress 45 degrees (30). Also, equilibrium is enforced in (31) using a relation similar to (22).

$$(30) \quad S_{45} = \frac{S_b(0)\sqrt{2}}{2}$$

$$(31) \quad \int S_{45} r \, dA_{45} = M_{res}$$

Where A_{45} is the cross-sectional area that is coincident with a radial line drawn 45 degrees into material gusset space from a gusset free edge. M_{res} was calculated for (22). The calculation of the coefficients I and J simply becomes the solution of two simultaneous equations given by (32) and (33).

$$(32) \quad I = \frac{12\,M_{res} - 3\sqrt{2}\,r_L^2\,t\,S_b(0)}{4\,r_L^3\,t}$$

$$(33) \quad J = \frac{\sqrt{2}\,S_b(0)}{2}$$

The development of angular stress distribution about a 45 degree axis is complete.

Until now, the stresses under consideration were specifically in-plane angular stresses about the origin of the gusset. There is also a radial stress that exists at the boundaries of the gusset space. This radial stress is nominally equal to the maximum beam bending stress at the gusset tip.

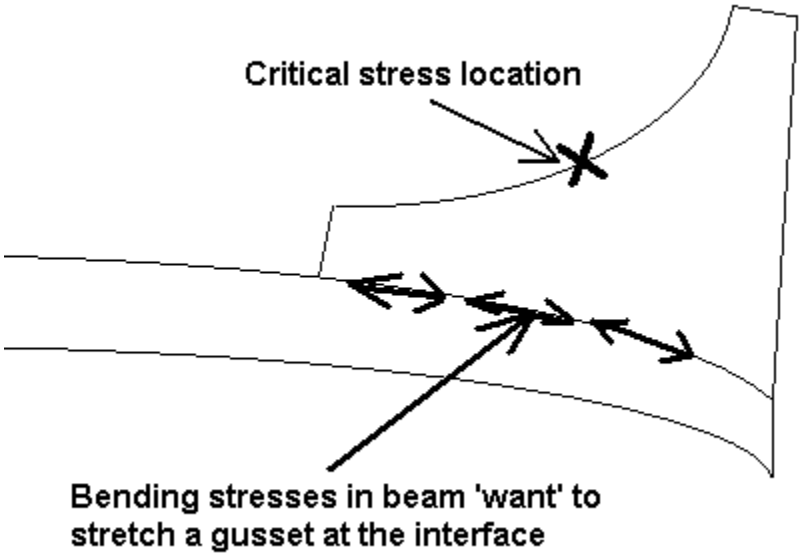

Figure 3.10: Beam bending

To a certain extent, it is acceptable to think of part of the gusset as just a part of the beam, but as the gusset height increases, it begins behaving independently from the beam. For this analysis, the total height of the gusset is key in determining the bending stress contribution to the critical location at the midpoint of the parabolic free edge. It is found, through numerical simulation and observation, that the beam bending stress contributes to the stress state following the relation given in (34).

$$S_{(b-applied)} = S_{(b-beam2)} 0.25^{\left(\frac{h_s}{h_{beam2}}\right)} \quad (34)$$

where h_{beam2} = height of the second beam (the second beam is the horizontal beam in figure 1). $S_{b\text{-}beam2}$ = strength of materials result for the average maximum bending stress in the second beam. h_s is the critical stress height given by (35).

$$(35) \quad h_s = r_L \sin\left(\frac{\pi}{4}\right)$$

The angular and radial stress components for a gusset have been described in the preceding section. The maximum angular stress result is equal to S_{rL}. The applied bending stress component is $S_{b\text{-}applied}$. The shear stress component will be neglected for this analysis. The stress state at the midpoint of the parabolic gusset free edge can now be constructed easily by superimposing the angular stresses given by (29), (32), and (33) and the bending stress contribution given by (34). The stress state at the gusset tip off of the toe of the weld is still not completely developed and will require additional study in chapters 4 and 5.

Chapter 4: Experimental Results and Discussion

The acquisition of weld metal elastic modulus was facilitated by micro-hardness testing with a Knoop indenter. The equipment used was a Buelher MicroMet indentation system. The indentations were prepared with a variety of indentation forces ranging from 200 grams force to 1000 grams force. It was observed that indentations made with more than 500 grams force resulted in indentations with 'wavy' edges and were subsequently removed from the data set. The results included were only derived from indentations created with 200 to 500 grams force. The specimens tested consisted of two 1⁄2 inch thick plates welded together at a 90 degree angle to form a T joint. The weld bead had a throat dimension of 0.25 inches. The parent material that was used was a mild steel (ASTM 1018). The welding wire was ER70S-6. The composition of the shielding gas was 95%Ar - 5%O. A 0.052 inch electrode was used with 28-30 Volts at 370-420 Amps. Weld wire was fed feed at 435-530 in/min. The specimen was sliced perpendicular to the direction of the weld bead to create a 1⁄2 inch thick slice. The freshly cut surface was ground and polished using several grit sanding and polishing papers. The final polishing disc used was a 30 micro-inch grit disc; the finish was very smooth. The next step was to etch the surface of the weld bead to positively identify the depth of penetration and to create boundaries for indentation. The specimen was then cut off near the welded joint so that it could fit into the micro indentation tester, then it was lightly polished again with 30 micro-inch paper. Figure 4.1 shows the cut off and polished sample.

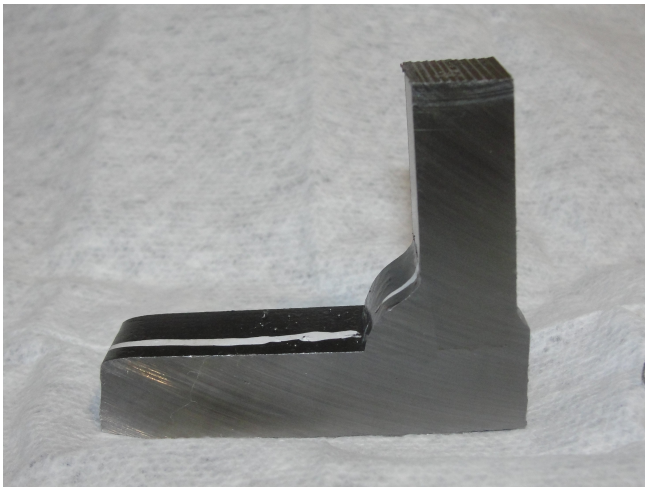

Figure 4.1: Welded specimen prepared for micro-indentation testing.

Observing the specimen in figure 4.1 closely, the boundaries of the weld are easy to see. Ten indentations were performed on three such samples. The long and short diagonals were measured for each indentation and the Knoop hardness number was recorded for each. The conversion of hardness and geometric data to elastic modulus is provided by Conway [1986]. Conway developed a method for calculating approximate elastic modulus by measuring the long and short diagonals of the diamond shaped Knoop indentation. His results are given by equation (36).

$$(36)\quad \left(\frac{b_R}{b_x}\right)^2 = 1-(2(1-\nu^2)\tan(\gamma))\frac{HKN}{E}$$

where E = elastic modulus, ν = Possion's ratio,
γ = average half angle of Knoop indenter (typically 75 degrees), b_R = measured short diagonal,
b_x = measured long angle divided by 7.11, HKN = Knoop hardness number.

The average calculated elastic modulus for weld metal was approximately 150 GPa. This result can now be used in the calculation of the dissimilar material corner singularity.

Chapter 5: Stress Analysis

Elastic mismatch is a source of local stress variation which can help characterize the interfacial stress distribution at a bonded joint. Elastic mismatch literature and peeling stress literature are very similar in that displacements of dissimilar bodies are set equal to each other and the resulting differential equation is solved. Timoshenko touched the concept of mechanical mismatch when studying the thermal mismatch in bimetallic thermostats [Timoshenko, 1925]. Since then, many solutions have used the thermal mismatch solution technique to study the effects of various mismatches in mechanical properties. Elastic mismatch is often encountered in the study of composite materials where stiffness varies from material to material. The stress field variations can be accounted using the solution techniques in Paranjpye, Beltz and MacDonald [2005]. Experimental and numerical studies have shown that the effects of elastic modulus mismatch can be significant in some cases. Welded joints inherently have elastic modulus mismatch built into them. Spot welded lap joints are very prevalent in elastic modulus mismatch literature; perhaps because of the prevalence of spot welded structures in automotive applications. In the case of an adhesive-plus-spot-welded lap joint examined in the paper by Darwish and Al-Samhan [2004], the free edge stresses vary as the elastic modulus of the adhesive varies. Although the author does not comment on this, the results are neatly graphed for three adhesives with unique elastic moduli. Analytical studies have been performed on similar lap joint geometries without the presence of the adhesive. The elastic modulus mismatch is slightly over- predictive of stresses in Lin and Pan [2008] because a spot weld is modeled as a rigid inclusion. The

motive and intention of finding a local stress concentration factor is preserved and local SCF's are derived from elasticity principles. The re-entrant corners inherent to these joints indicate that singular stress fields may be present. Re-entrant corner stress fields can be evaluated using an eigenfunction strategy [Richards, 2001]. Additional papers combine the mismatch and corner singularity effects to determine the variation in a local stress field in a bi-material corner [Bogy, 1971; Zhang 2003]. Using the eigenfunction expansion technique for a bi-material joint (e.g. steel and weld metal) will require that the eigenvalues and stress intensity factor be calculated using analytical contour integrals or numerical methods. Semi-analytical methods are preferred here because of path independence issues which help ensure a precise stress intensity factor. Qian and Akisanya [1999] take a unique approach to finding stress intensity factors using finite element methodology that are very similar to those acquired through other numerical methods. For a well trained engineer, path dependence can be dealt with using simpler methods, like the one provided in the text by Sanford [2003], which involves linearly extrapolating apparent stress intensity factors using numerical simulation. Between elastic modulus mismatch and re-entrant corner singular stresses, an effective analytical model is developed.

A typical fillet weld profile can be roughly approximated by a straight sided free edge. The location where the free edge intersects base metal is typically the location of interest as far as stress determination and fatigue evaluation are concerned. That location is marked with an 'X' in figure 5.1.

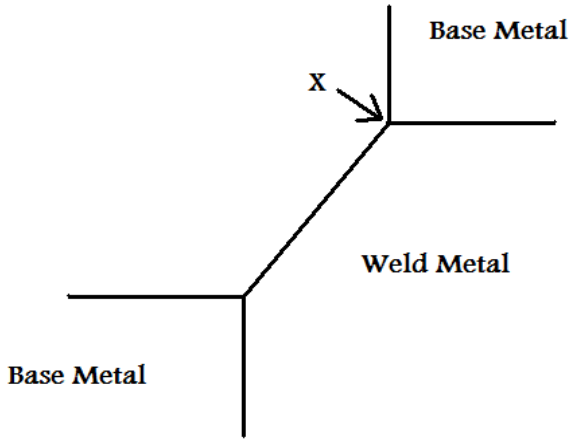

Figure 5.1: Critical stress location

The problem is conveniently set up so that existing elastic mismatch methods from literature can help determine the critical stress magnitudes. Figure 5.2 shows the critical stress location more closely.

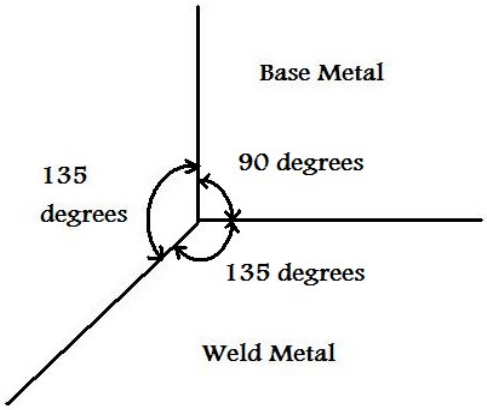

Figure 5.2: Local geometry of weld fillet–base metal interface

Notice, in figure 5.2, that the total angle of opening in the joint is 135 degrees. This angle of opening only corresponds to a fillet weld joining two parent material parts at right angles. If the parent material parts are oriented differently, than the opening angle will be different, and the resulting eigenvalues (and eventually, the stress solution) will be

different. It is advantageous at this point to develop some notation regarding components of this opening angle. The subscript 1 will denote base metal characteristics, the subscript 2 will denote weld metal. Therefore, θ_1 will correspond to the 90 degree angle shown in figure 3. θ_2 will correspond to the 135 degree angle within the base metal space in figure 5.2. The ψ axis equals zero at the material interface and is positive in the counterclockwise direction in figure 5.2.

Williams [1959] solution of a single ended crack in dissimilar media provides a basis for determining the severity of the stress singularity at a bimaterial re-entrant corner. The solution is very similar to a homogeneous wedge problem, and can be solved for the single material case easily, as demonstrated in Williams literature. The problem is solved by the complex stress function $r^{\lambda+1} F_n(\psi)$,

Where $F_n(\psi)$ s given by (37).

$$(37) \quad F_n(\psi)=a_n \sin(\lambda+1)\psi+b_n \cos(\lambda+1)\psi+c_n \sin(\lambda-1)\psi+d_n \cos(\lambda-1)\psi$$

$F_1(\psi)$ and $F_2(\psi)$ are stress functions of base metal and weld metal respectively. Equilibrium equations are set up for both materials, including equal displacement relations at the material interface. The free edge boundaries are given by (38).

$$(38) \quad F_1\left(\frac{\pi}{2}\right)=F'_1\left(\frac{\pi}{2}\right)=F_2\left(\frac{3\pi}{4}\right)=F'_2\left(3\frac{\pi}{4}\right)=0$$

Boundary conditions at the interface are given by (39), (40), (41), and (42).

$$(39) \quad F_1(0)=F_2(0)$$

$$(40) \quad F'_1(0)=F'_2(0)$$

$$(41) \quad \frac{1}{2\mu_1}(-F'_1(0)-4c_1(1-\sigma_1))=\frac{1}{2\mu_2}(-F'_2(0)-4c_2(1-\sigma_2))$$

$$(42)\quad \frac{1}{2\mu_1}(-(\lambda+1)F_1(0)-4d_1(1-\sigma_1))=\frac{1}{2\mu_2}(-(\lambda+1)F_2(0)-4d_2(1-\sigma_2))$$

These eight equations carry eight unknowns along with the constant λ. In order for this system of equations to yield a non-trivial solution, λ must be defined so that the det[M] = 0, where M is the 8x8 matrix carrying the terms of the above eight equations. As Williams indicated in his paper, for the case where $\theta_1 = -\theta_2$. λ has no solution between 0 and 1 if the materials are dissimilar. Therefore, it was necessary to define λ as a complex eigenvalue, $\lambda = \lambda_R + i\lambda_i$. However, since θ_1 and θ_2 are different values than what is seen in Williams, 1959, it is still possible that real eigenvalues exist between 0 and 1. The methodology used by Qian and Akisanya [1999] in which a characteristic equation is solved for eigenvalues, is a very simple method that will be used for this analysis. As a note, if the only eigenvalues between 0 and 1 were complex, then the analysis would turn to the methodology presented in Carpinteri and Paggi [2007]. The aforementioned have developed a method for calculating eigenvalues numerically using the condition of the equilibrium matrix. The solution involves finding singular instances in the condition calculation of the equilibrium matrix and finding what real and imaginary eigenvalue parts correspond to those instances. This method was used along with the one used in Qian and Akisanya [1999]. Both methods resulted in the same smallest positive eigenvalue of $\lambda_1 = 0.583$. There exist higher order eigenvalues, however they will be neglected for the purposes of this analysis. Since a complex polar stress function of the form $r^{\lambda+1} F_n(\psi)$ results in a radial, angular, and shear stress components proportionate to the form $r^{\lambda-1}$, any eigenvalue with $0<\mathrm{Re}\,\lambda < 1$ yields a singular stress field. This is important in understanding the reasons behind the mathematical singularity as well as for calculating the numerical stress intensity factor.

The next step is to quantify stress intensity factors that exist at this joint. It is known that the stress intensity factor for cracked media is proportional to the applied nominal stress due to the linear nature of fracture mechanics. The stress intensity factor is also proportional to a geometric shape factor which is unique for all geometries. The stress intensity factor is given by (43).

$$(43) \quad K_1 = \sigma_{applied} a^{(1-\lambda_1)} Y_{shape}$$

where $\sigma_{applied}$ = nominal combined applied stress, Y_{shape} = geometric shape factor, K_1 = stress intensity factor, $a = l_{tip}/2$

From numerical extrapolation studies based on the methods found in (Sanford, 2003), Y_{shape} for this particular geometry is found in (44).

$$(44) \quad Y_{shape} = 0.826$$

In application of the Sanford [2003] method, ANSYS® Advanced Academic Research, version 12.1, was used. The method aims to collect nodal stress or displacement results over a path approaching the re-entrant corner (the text requires that the path approaches a crack tip, but the appropriate modification is made). The apparent stress intensity factor is calculated by providing a best fit line through the linear portion of the stress or displacement gradient leading up to the corner. The apparent stress intensity factor is calculated to be the Y-intercept of the best fit line through the linear data. A 3-d solid finite element model was created. For the re-entrant corner geometry, solid187 elements with a collapsed node on two parallel faces were used to create the singular stress behavior. The element edge length for the local mesh was 0.01 inches with an aspect ratio of nearly 1. In figure 5.3, the geometry is divided into two bodies. The body near the top of figure 5.3 has the elastic material properties of steel ($\nu = 0.3$, $E = 205$ GPa).

The body near the bottom of figure 5.3 has the material properties of weld metal as measured earlier (ν=0.3, E=152.75 Gpa). The above shape factors were calculated and checked for validity after apparent stress intensity factors were obtained using Sanford's extrapolation technique.

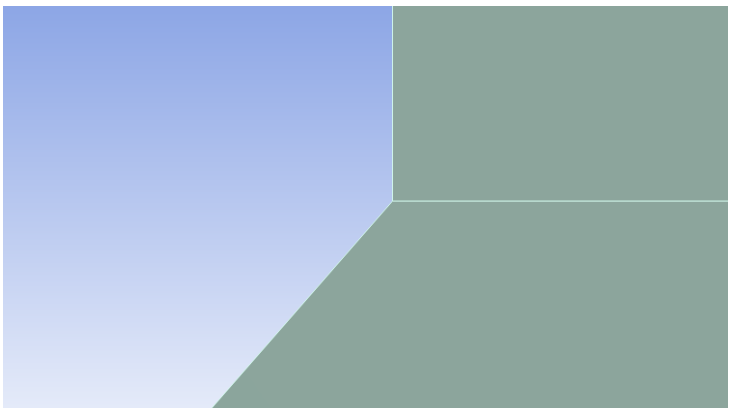

Figure 5.3: Geometry for numerical study.

It can be observed that the typical fillet weld geometry has two corners of dissimilar material. Figure 5.4 shows these locations as location 1 and location 2. When beam bending stresses are much larger than gusset angular stresses, location 1 is typically in more danger of fatigue fracture. When the angular gusset stresses are much larger than the beam stresses, then location 2 is more likely to fracture first. Finally, when the bending and gusset angular stresses are the same, the two fillet corners are equally affected. Therefore, there is much benefit in using a combined applied stress in the determination of the stress intensity factors. Since the geometries are identical in the near field regions of 1 and 2, the stress intensity factor calculated above will automatically represent the worse of the two fillet corners. The applied stress will be dominated by the greater of the two stress components.

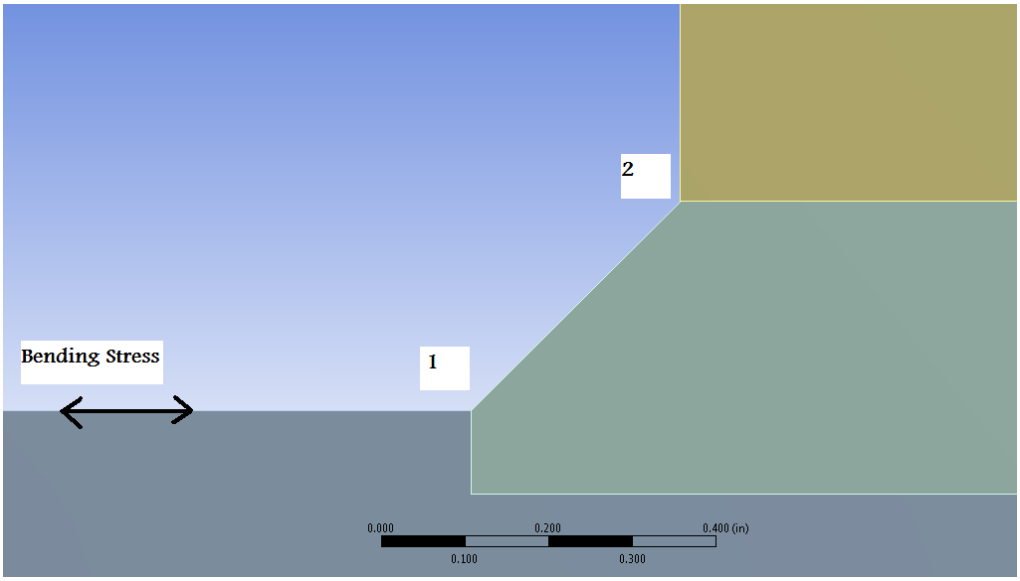

Figure 5.4: Critical Locations 1 and 2. The material on the top and bottom is steel, the center material is weld metal.

K_1 can be determined for any loading for this type of geometry. Here, the stress intensity factors may be compared to critical stress intensities for weld metal to determine if fracture is eminent. This may be the preferred method for evaluating a corner like this, but critical fracture parameters for weld metal interfaces are sparse in literature. There are, however, data in the stress-life domain which would help an engineer determine if crack initiation is likely after *n* cycles. These stress intensity factors and eigenvalues will have to be substituted back into a stress solution like Williams [1959], or Qian and Akisanya [1999]. Solving for the stress distribution here would be redundant. Qian and Akisanya [1999] have the entire solution clearly outlined in an appendix. See the example problem in chapter 6 for relevant coefficients from Qian and Akisanya [1999]. Using the singular stress field to predict crack initiation would likely entail using Dang Van and Fermer's principles or other industrial methods.

Chapter 6: Design Application

One intention behind the writing of this paper is to provide theoretical and empirical tools to an engineer so that he or she may perform better in the field of mechanical frame design. This section specifically describes how to implement these tools. To begin, it must be noted that the gusseted welded connection is tricky since, until now, there were no methods for determining gusset boundary conditions for design engineers, but also because the fatigue criteria at the weld and base metal inherently differ. In the case of mild steels, the endurance limit for base metal is typically 1.5 to 2 times greater than that of a fillet weld. Therefore, a gusset can be stressed up to 2 times higher than its welded boundary. Despite the complications of disparate failure criterion, the optimal design with regards to minimizing weight can be achieved through the manipulation of just a few key variables. Heading back to the gusseted frame shown in figure 1.3 and again here in figure 6.1, it must be realized that the beams must be designed with the knowledge that stress intensity factors will not allow the beams to maintain nominal strength of material stresses over their entire spans.

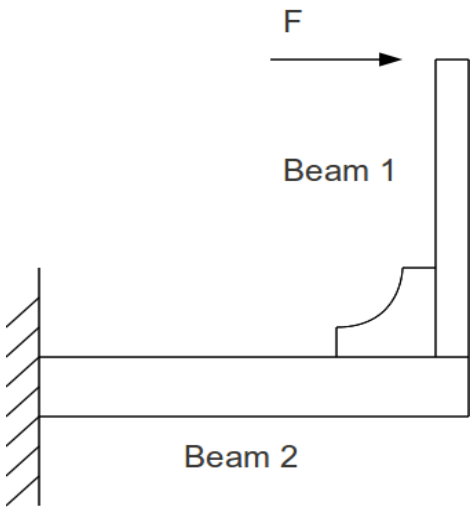

Figure 6.1: Gusseted frame.

Referring to figure 6.1, it is immediately seen that the bending stress in beam 1 increases with the distance from the applied force until the gusset tip meets the beam. Therefore, an engineer should choose design stresses against a fatigue criteria using the nominal bending stresses at the gusset tip location on beam 1. To anticipate the effects of the stress singularity at the gusset tip, an engineer should select a beam with a slightly higher section modulus than a beam suited for nominal bending stresses. This should serve as the first design point for beam 1. Similarly, for beam 2, although the bending stresses are nominally constant over the span, the engineer should choose a slightly over sized beam in anticipation of the effects of the stress singularity at the gusset tip.

Regarding the design of the parabolic gusset, there are three variable to work with. The thickness of the plate, the leg length, and the gusset tip height. Gusset tip height can be removed from consideration because of the formulation of gusset tip stresses. Thinking critically about the development of equation (27), it is known that larger l_{tip} values result in larger S_{tip} values, which, in turn, enter into the singular corner. It is logical to reduce the stresses that enter into the corner singularity. Therefore, it is appropriate to make l_{tip}

as small as possible. Ideally, l_{tip} would be zero, however, issues such as weld burn through prevent this from happening. Therefore, the weld size, gusset thickness, and welding method will determine what the minimum gusset tip height will be.

Thickness is another easily manipulated variable. As a general rule of thumb, large thin gussets almost always perform better than small thick gussets in fatigue . Therefore, an engineer should start thin. It will be known immediately if the gusset is too thin because stresses at the mid-point of the parabolic free edge will be too high relative to fatigue or plate buckling criterion. An engineer should iterate the gusset thickness to be as thin as possible while maintaining acceptable mid-free-edge stresses in order to utilize all available material efficiently.

At this point, gusset leg length is the only design variable left to manipulate. It is advised to iterate leg length until weld toe stresses off of the gusset tip are acceptable according to a weld fatigue criteria. The optimal design of the L-shaped gusseted frames under fatigue loads is easily converged upon if the methodology in this paper were automated in a common spreadsheet software.

An example solution of gusset tip stresses has been included to highlight the utility of this work. The results from this work have also been correlated with FEA results taken from ANSYS®. Consider a mechanical frame (figure 6.1) cyclically loaded by a pseudo-static load of 100 lbf. The frame consists of two beams connected perpendicularly to form an L frame. Beam 1 is a 1 inch wide x 1 inch tall x 14 inch long beam. Beam 2 is a 1 inch wide x 1.5 inch tall x 15 inch long beam. A parabolic gusset supplements the connection between the two beams. The gusset has leg lengths of 5 inches and a tip height of 0.5 inches. The gusset plate is 0.25 inches thick. The beams and the gusset are both made of

steel (elastic modulus, E = 2.9x10^7 psi, Poisson's ratio, υ = 0.3).

Using the methodology presented earlier, to find the gusset tip stresses, the stresses at the gusset-beam interface should be determined first. The coefficients for the cubic stress function at the interface are found to be the following:

$$P = -102.959 \frac{lbf}{inch^2}$$
$$M = 4.625 \frac{lbf}{inch^5}$$
$$N = -117.743 \frac{lbf}{inch^4}$$
$$O = 513.725 \frac{lbf}{inch^3}$$

The nominal stress at the gusset tip due to gusset pull-out is 100.254 psi. The bending stress from a strength of materials approach in beam 2 is 3733 psi. Therefore, two components of normal stress are defined. The resultant normal stress is 3833 psi, this will be the applied stress in the determination of the stress intensity factor for the singular stress field. Plane strain conditions are assumed for the determination of the stress singularity at the weld toe. The stress intensity factor calculated for an eigenvalue of 0.583, a shape factor of 0.826, and a = l_{tip}/2 is calculated as follows.

$$K = \sigma_{applied}\, a^{(1-\lambda)}\, Y_{shape} \quad therefore,$$
$$K = 3738\, psi\, (0.25\, inch)^{(1-0.583)} (0.826)$$
$$K = 1732\, psi\, inch^{(1-0.583)}$$

The stresses on the top of beam 2 leading up to the toe of the weld can be calculated by following Williams [1959]. It is noted that for welded mild steel joints where a fillet weld is idealized to take a 45 degree departure away from the base metal surface, the stresses on the free edge of the base metal always take the form given by (45):

$$(45) \quad \sigma = K_1 r^{(\lambda-1)} f_{r1}$$

Where f_{r1} = 1.195 and r = the radial distance from the weld toe along the base metal free edge. Therefore the stress distribution leading up to the weld toe follows this compact relation:

$$\sigma = 1732\ psi\ inch^{(1-0.583)}\ r^{(0.583-1)}\ 1.195$$

The following is a plot of the stress on the free edge of the beam. As expected, the asymptotic solution is inaccurate far away from the weld toe. This is seen in figure 6.2.

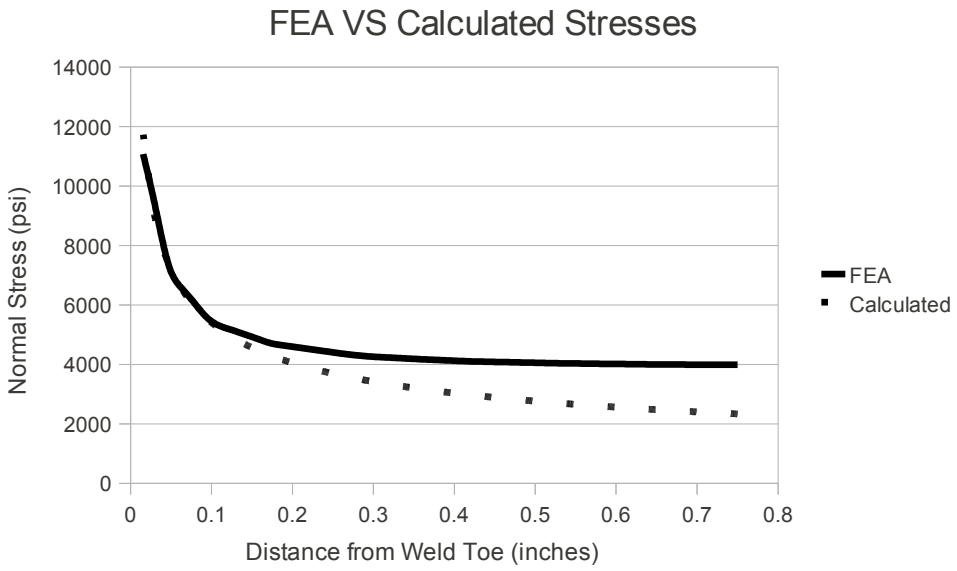

Figure 6.2: Calculated stresses compared to FEA stresses off of weld toe on beam free edge.

The stresses in the near field region of the weld toe correlates very well with FEA results as seen in figure 6.3.

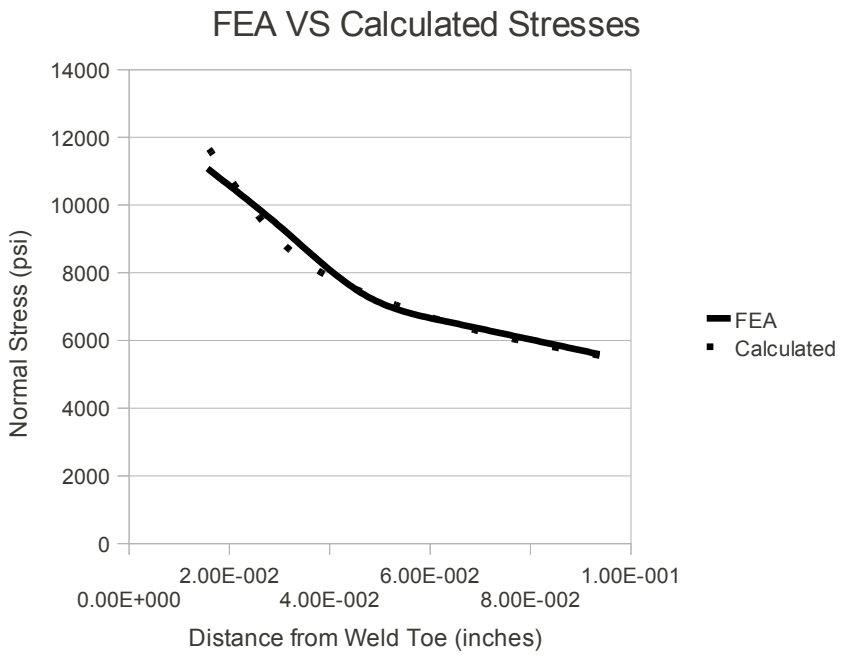

Figure 6.3: Calculated stresses compared to FEA stresses on beam free edge in a near field region to the weld toe.

The stress distribution due to the singularity can now be entered into any common industrial fatigue method to predict fatigue crack initiation.

Chapter 7: Conclusions and Future Work

From the current work, several important design concepts and strategies have been observed. When designing welded gusseted frames subject to fatigue loading,

1) It is important to slightly oversize beams based on strength of materials methods.
2) Gusset tip heights on parabolic gussets should be made as small as possible while avoiding weld burn-through.
3) Gusset thickness should be based on the stresses at the midpoint of the parabolic free edge.
4) Gusset leg length will likely be the only design variable that will require iteration until an optimally light design is achieved.
5) Interfacial beam-gusset stresses are given in equations (19) and (24 – 26).
6) Stresses on the midpoint of a parabolic free edge are given by equations (29) and (32 - 34).
7) The stress distribution near the weld toe is given by equations (43 = 45).

It is also learned that using relative load path stiffness to determine load path intensities in complicated plate geometry is a good method to use when attempting to approximate a difficult stress solution.

Using the method of load path determination for in-plane loading in plates can greatly simplify the search for appropriate boundary conditions when features or defects in a plate are large enough to perturb nominal boundary conditions. This new method for determining boundary loads can be used when cuts in plates are too numerous or close to boundary conditions and traditional boundary perturbation methods become too

cumbersome to use effectively in a design situation. It is recommended that the load path stiffness method be developed further so that a useful and simple tool can be available to design engineers to determine contact stresses and boundary loads.

The material property study and the results for weld metal modulus are inherently limited. There are many different weld processes, wire types, base metal types, and environmental factors that make additional testing of welded joint material properties necessary. The results here should be followed by changing the base metal to something with more carbon; something more heat treatable. The stiffness of the weld metal – steel slurry was more flexible than expected, future research should examine how that changes with more carbon in the mixture. Concurrently, stress intensity factors should be updated as more weld metal material properties are tested and published.

After cantilevered L frame design is firmly established, other configurations of boundary conditions and frame geometry should be evaluated for usable stress solutions. Some specific examples are 1) simply supported T frames 2) L frames loaded with a concentrated moment 3) L and T frames with combine loading, and 4) the confounding case where a frame is subject to torque where the gusset is forced to respond to out-of-plane loading. Many geometric frame configurations are found in common machine design and there is no shortage of opportunities for researchers in academia or industry to solve for unknown stress solutions.

References

ANSYS® Academic Research, Release 13.0, Help System, *Theory Reference,* ANSYS, Inc.

Ashby, M. F. *Materials Selection in Mechanical Design*. Amsterdam: Butterworth-Heinemann, 2005. Print.

Bogy, D. "Stress Singularities at Interface Corners in Bonded Dissimilar Isotropic Elastic Materials." *International Journal of Solids and Structures* 7.8 (1971): 993-1005. Print.

Boyce, B. L., P. L. Reu, and C. V. Robino. "The Constitutive Behavior of Laser Welds in 304L Stainless Steel Determined by Digital Image Correlation." *Metallurgical and Materials Transactions A* 37.8 (2006): 2481-492. Print.

Carpinteri, A., and M. Paggi. "Analytical Study of the Singularities Arising at Multi-material Interfaces in 2D Linear Elastic Problems." *Engineering Fracture Mechanics* 74.1-2 (2007): 59-74. Print.

Chung, K., W. Lee, J. Kim, C. Kim, S. Park, D. Kwon, and K. Chung. "Characterization of Mechanical Properties by Indentation Tests and FE Analysis %u2013 Validation by Application to a Weld Zone of DP590 Steel." *International Journal of Solids and Structures* 46.2 (2009): 344-63. Print.

Conway, J. C. "Determination of Hardness to Elastic Modulus Ratios Using Knoop Indentation Measurements and a Model Based on Loading and Reloading Half-cycles." *Journal of Materials Science* 21.7 (1986): 2525-527. Print.

Darwish, S. "Design Rationale of Weld-bonded Joints." *International Journal of*

Adhesion and Adhesives 24.5 (2004): 367-77. Print.

Genevois, C., A. Deschamps, and P. Vacher. "Comparative Study on Local and Global Mechanical Properties of 2024 T351, 2024 T6 and 5251 O Friction Stir Welds." *Materials Science and Engineering: A* 415.1-2 (2006): 162-70. Print.

Hibbeler, R. C. *Mechanics of Materials*. Upper Saddle River, NJ: Pearson Prentice Hall, 2005. Print.

Jou, Min. "Experimental Study and Modeling of GTA Welding Process." *Journal of Manufacturing Science and Engineering* 125.4 (2003): 801. Print.

Kaelble, D. H. "Theory and Analysis of Peel Adhesion: Bond Stresses and Distributions." *Journal of Rheology* 4.1 (1960): 45. Print.

Kartal, M., Rafal M. Molak, Mark Turski, S. Gungor, Michael E. Fitzpatrick, and Lyndon Edwards. "Determination of Weld Metal Mechanical Properties Utilising Novel Tensile Testing Methods." *Applied Mechanics and Materials* 7-8 (2007): 127-32. Print.

Kong, F., M. You, X. Zheng, and H. Yu. "Three-dimensional Stress Analysis of Adhesive-bonded Joints under Cleavage Loading." *International Journal of Adhesion and Adhesives* 27.4 (2007): 298-305. Print.

Lin, P., and J. Pan. "Closed-form Structural Stress and Stress Intensity Factor Solutions for Spot Welds under Various Types of Loading Conditions." *International Journal of Solids and Structures* 45.14-15 (2008): 3996-4020. Print.

Lockwood, W., B. Tomaz, and A. Reynolds. "Mechanical Response of Friction Stir Welded AA2024: Experiment and Modeling." *Materials Science and Engineering A* 323.1-2 (2002): 348-53. Print.

Maier, P., A. Richter, R. G. Faulkner, and R. Ries. "Application of Nanoindentation Technique for Structural Characterisation of Weld Materials." *Material Characterization* 48.4 (2002): 329-39. Print.

Malek, Amir M., Hamed Saadatmanesh, and Ehsani R. Mohammad. "Prediction of Failure Load of RC Beams Strengthened with FRP Due to Stress Concentration at Plate End." *ACI Structural Journal* 95.1 (1998). Print.

Ndiaye, A., S. Hariri, G. Pluvinage, and Z. Azari. "Stress Concentration Factor Analysis for Welded, Notched Tubular T-joints under Combined Axial, Bending and Dynamic Loading." *International Journal of Fatigue* 31.2 (2009): 367-74. Print.

Paranjpye, Alok, Glenn E. Beltz, and Noel C. MacDonald. "An Analytical Model for the Effect of Elastic Modulus Mismatch on Laminate Threshold Strength." *Modelling and Simulation in Materials Science and Engineering* 13.3 (2005): 329-40. Print.

Popov, G. Ia, and L. Ia Tikhonenko. "Exact Solution of Plane Problems on the Contact between Semi-infinite Beams and an Elastic Wedge." *PPM* 39.6 (1975): 1100-109. Print.

Popov, G. Ia, and L. Ia Tikhonenko. "Two-dimensional Problem of the Contact between a Semi-inifinite Beam and an Elastic Wedge." *PPM* 38.2 (1974): 312-20. Print.

Richards, Rowland. *Principles of Solid Mechanics*. Boca Raton, FL: CRC, 2001. Print.

Sanford, R. J. *Principles of Fracture Mechanics*. Upper Saddle River, NJ: Prentice Hall, 2003. Print.

Stratford, T., and J. Cadei. "Elastic Analysis of Adhesion Stresses for the Design of a Strengthening Plate Bonded to a Beam." *Construction and Building Materials* 20.1-2 (2006): 34-45. Print.

Sutton, M., B. Yang, A. Reynolds, and J. Yan. "Banded Microstructure in 2024-T351 and 2524-T351 Aluminum Friction Stir WeldsPart II. Mechanical Characterization." *Materials Science and Engineering A* 364.1-2 (2004): 66-74. Print.

Timoshenko, S. "Analysis Of Bi-Metal Thermostats." *Journal of the Optical Society of America* 11.3 (1925): 233. Print.

Timoshenko, Stephen, and J. N. Goodier. *Theory of Elasticity, by S. Timoshenko and J. N. Goodier,... 2nd Edition.* New York-Toronto-London: McGraw-Hill Book, 1951. Print.

Williams, M. L. "On the Stress Distribution at the Base of a Stationary Crack." *Journal of Applied Mechanics* 24 (1957): 109-14. Print.

Williams, M. L. "The Stresses around a Fault or Crack in Dissimilar Media." *Bulletin of the Seismological Society of America* 49.2 (1959): 199-204. Print.

Wu, Zhigen, and Yihua Liu. "Asymptotic Fields near an Interface Corner in Orthotropic Bi-materials." *International Journal of Fracture* 156.1 (2009): 37-51. Print.

Zhang, H. "Hamiltonian Principle Based Stress Singularity Analysis near Crack Corners of Multi-material Junctions." *International Journal of Solids and Structures* 40.2 (2003): 493-510. Print.

Zheng, L., D. Petry, H. Rapp, and T. Wierzbicki. "Characterization of Material and Fracture of AA6061 Butt Weld." *Thin-Walled Structures* 47.4 (2009): 431-41. Print.

Acknowledgements

I would like to thank my Major Professor, Dr. Palaniappa A. Molian for providing excellent guidance while giving me the freedom to pursue a project which was outside of his current area of research. I would also like to thank my committee members, Dr. Pranav Shrotriya, and Dr. Fouad Fanous, for challenging me to create a theoretical basis for the welded frame design problem.

There are several people in my academic and professional careers who helped me find my path. Dr. Rebecca Dupaix of The Ohio State University introduced me to stress analysis and FEA in a research setting. Dr. Mendelsohn, also at Ohio State, spent many hours tutoring me on the methods of complex potentials in fracture mechanics. Bob Kephart, Materials Specialist - Vermeer Corporation, trained me to perform rheological and other material studies in his lab. He specifically helped me with the knoop microhardness testing for this thesis. For that, I am very thankful. Dave Landon, Weld Engineering Manager - Vermeer Corporation, lent me some of his vast welding engineering knowledge which really kept my research moving. Darrel Wiley, Structural Analyst, and Tom Haley, Product Safety Manager, both at Vermeer Corporation, have been recommending parabolic gussets for years, and it is because of them that I became interested in finding a theoretical stress result for such an abnormal geometry.

I would like to thank my mother and father for raising me, supporting me, and making me who I am today. I would like to thank my wife, Muniba, for showing what hard work and determination really look like. Finally, I would like to thank the Most High for giving me the strength and will to do something good in this world.